Structural Study of Amorphous Alloys with a Wide Supercooled Liquid Region by the Anomalous X-ray Scattering (AXS) Method

Structural Study of Amorphous Alloys with a Wide Supercooled Liquid Region by the Anomalous X-ray Scattering (AXS) Method*

Eiichiro Matsubara and Yoshio Waseda

Research Institute of Mineral Dressing and Metallurgy (SENKEN)

(Received February 1, 1992)

Synopsis

The atomic structures of new kinds of as-quenched $La_{55}Al_{25}Ni_{20}$ and $Zr_{60}Al_{15}Ni_{25}$ amorphous alloys exhibiting a wide supercooled liquid region and a high reduced glass transition temperature have been studied with the anomalous x-ray scattering (AXS) method in combination with the ordinary x-ray diffraction. The environmental structures around certain constituent elements in the alloys were determined with the AXS method. The atomic structures of these amorphous alloys annealed in the super-cooled liquid region were also investigated. The systematic structural studies revealed a structural feature common to these amorphous alloys. Namely, the environment around a certain element in the amorphous sample is very different from that in the crystallized sample. Such as, Ni atoms around La atoms in $La_{55}Al_{25}Ni_{20}$ and Al atoms around Zr atoms in $Zr_{60}Al_{15}Ni_{25}$. In other words, quite a large change of the environments around a certain element is required for the crystallization, which controls the crystallization in these amorphous alloys. Consequently, This may provide a high thermal stability of these amorphous alloys.

I. Introduction

Oxide glasses have a wide supercooled liquid region and show a high thermal stability, which enables us to deform these oxide glasses into desired shapes and to use them as practical materials. However, most of metallic amorphous alloys show no glass transition temperature (T_g). Only a few Pt- and Pd-based amorphous alloys, such as Pt-Ni-P, Pd-Ni-P, Pd-Cu-Si, Pd-Ni-Si etc., have been reported to have a wide supercooled liquid region[1]. Quite recently, Inoue *et al.* have discovered the lanthanide-aluminum based amorphous alloys, such as La-Al-Ni[2] and La-Al-Cu[3] having a wide supercooled liquid region comparable to that for Pt-Ni-P amorphous alloys[4]. Furthermore, Inoue *et al.*[5] have found other amorphous alloys with a wide supercooled liquid region in Zr-Al-TN (TN = Mn, Fe, Co, Ni or Cu) systems which include neither noble metals nor

---

* 92-R6*th* Report of the Research Institute of Mineral Dressing and Metallurgy (SENKEN)

lanthanide metals. This is quite promising for application to practical materials.

Presence of a high resistance to the nucleation and growth of crystalline phases, and strong bonding among constituent elements etc. has been suggested by Inoue *et al.*[2,3,5] in order to explain the origin of a wide supercooled liquid region and high glass-forming capacity in these new metallic amorphous alloys. The details, however, have not been well understood yet. The authors have studied the atomic structures of these new amorphous alloys by the anomalous x-ray scattering (AXS) method as well as the ordinary x-ray diffraction. One of the common features in these amorphous alloys is that the atomic sizes of the three constituent elements are different each other[2,5]. For example, La (0.187 nm), Al (0.143 nm) and Ni (0.124 nm) in the La-Al-Ni system. This makes the analysis of these amorphous alloys by the ordinary x-ray diffraction extremely difficult, in spite of the quite large differences among their x-ray atomic scattering factors. Because of such difference of their atomic sizes, no distinct first peak is observed in the profile of the ordinary radial distribution function (RDF) which is a sum of the six partial RDFs in the ternary system. Thus, by the ordinary x-ray diffraction, even the structural parameters in the nearest neighboring pairs can not be obtained. The environmental RDF for a certain constituent element determined by the AXS method may provide us more information of the atomic structures in the present systems.

In the present paper, the results of the structural studies in the $La_{55}Al_{25}Ni_{20}$ and $Zr_{60}Al_{15}Ni_{25}$ amorphous alloys will be presented and the origin of a wide supercooled liquid region will be discussed. Incidentally, the atomic concentrations selected in the present measurements give the largest temperature span ΔT_x in each system[2,5] which is defined as the difference between the crystallization temperature T_x and the glass transition temperature T_g.

II. Experimental

An ingot of the ternary alloy with a nominal composition of 55 at.% La, 25 at.% Al and 20 at.% Ni was prepared by arc-melting a mixture of pure lanthanum (99.9 wt%), aluminum (99.99 wt%) and nickel (99.9 wt%) in a purified argon atmosphere. From the master ingot, $La_{55}Al_{25}Ni_{20}$ amorphous ribbons of about 0.02 mm thickness and 1 mm width were produced by a single-roller melt-spinning technique in an argon atmosphere. Similarly, $Zr_{60}Al_{15}Ni_{25}$ amorphous ribbons were prepared, using pure zircon (99.9 wt%), aluminum (99.99 wt%) and nickel (99.9 wt%). Details of the sample preparation are described elsewhere[2,5]. Some of the ribbons were sealed in vacuum and annealed at a low temperature, so as to study the structural change of the as-quenched amorphous alloys due to low-temperature annealing. Others were crystallized by annealing for extremely long time in the supercooled liquid region so that the structural change due to the crystallization was also investigated. These annealing conditions are summarized in **Table 1** with the values of T_g, T_x and ΔT_x determined from the calorimetric studies by Inoue *et al.*[2,5] For x-ray measurements, the ribbons were cut into small pieces of about 20 mm long, closely arranged and fixed on an aluminum frame with a window of about 15 mm wide and 10 mm high for the x-ray measurements. In order to obtain enough scattering intensity from these ribbons, several layers were stacked up on the frame.

The ordinary x-ray scattering measurement was carried out with monochromatic Mo Kα-radiation produced by a molybdenum sealed x-ray tube in the operation of 40 kV and 20 mA and

Table 1 Summary of the annealing conditions of the as-quenched samples used in the present study, with the values of their glass transition temperature (T_g), crystallization temperatures (T_x) and temperature span ΔT_x ($= T_x - T_g$).

As-quenched samples	Annealing conditions	
	Temperature	Time
$La_{55}Al_{25}Ni_{20}$ (T_g=481 K, T_x=546 K, ΔT_x = 67 K)	418 K	10.8 ks (3 hrs)
	488 K	1.8 ks (30 min)
	510 K	300 s (5 min)
	510 K	360 ks (100 hrs)*
$Zr_{60}Al_{15}Ni_{25}$ (T_g=693 K, T_x=770 K, ΔT_x = 77 K)	730 K	120 s (2 min)
	730 K	180 ks (50 hrs)*

* The annealing conditions for crystallization of the amorphous samples.

a singly-bent graphite monochromator in diffracted beam. After the corrections for air-scattering, absorption and polarization, the observed intensity was converted into electron units per atom with the generalized Krogh-Moe-Norman method[6] using the x-ray atomic scattering factors[7], including the anomalous dispersion terms. The Compton scattering was corrected using the theoretical values[8] with the so-called Breit-Dirac recoil factor. Finally, the interference function $Qi(Q)$ was computed from this coherent scattering intensity, $I_{eu}(Q)$.

$$Q\,i(Q) = \frac{Q(I_{eu}(Q) - \sum_{j=1}^{N} x_j f_j^2)}{(\sum_{j=1}^{N} x_j f_j)^2} \qquad (1)$$

where $Q = 4\pi\sin\theta/\lambda$, θ is the scattering angle and λ the wavelength. The terms of x_j and f_j correspond to the atomic concentration and the atomic scattering factor of the element j and N the total number of the constituent elements (equal to 3 in the present case). The ordinary RDF which represents the radial distribution around the average atom was computed from the Fourier transformation of the function $Qi(Q)$.

$$4\pi r^2\rho(r) = 4\pi r^2\rho_o + \frac{2r}{\pi}\int_0^{\infty} Qi(Q)\sin(Qr)\,dQ \qquad (2)$$

where $\rho(r)$ is the radial number density function and ρ_o the average number density.

The AXS measurements were carried out at a beam line (6B station) with synchrotron radiation in the Photon Factory of the National Laboratory for High-Energy Physics, Tsukuba, Japan. The AXS measurements were made at Ni K-absorption edge in the $La_{55}Al_{25}Ni_{20}$ alloys and at Ni and Zr K-absorption edges in the $Zr_{60}Al_{15}Ni_{25}$ alloys. The incident energies on the lower energy side of the absorption edge were used in the present AXS measurements because at the

higher energy side of the absorption edge there exist extremely intense fluorescent radiations from the sample and particular near-edge phenomena, such as EXAFS and XANES which prevent us from evaluating the accurate values of the anomalous dispersion terms and the absorption coefficients. Also, by using the lower energy side of the absorption edge, the AXS equations were extremely simplified. All the measured intensities were corrected and converted into electron units per atom by the method explained above in the ordinary x-ray diffraction. Most of the physical constants except the anomalous dispersion terms were obtained from the same references introduced above. The anomalous dispersion terms in the vicinity of the absorption edges were theoretically calculated[9] with Cromer and Liberman's scheme[10]. The agreement between the experimental and theoretical values of the anomalous dispersion terms on the lower energy side of the absorption edge has been confirmed[11]. The details of the experimental setting and analysis are explained elsewhere[12]. Only some necessary equations for the following discussion will be given below.

When the anomalous x-ray scattering occurs with respect to an element of A in the system, the total x-ray atomic scattering factor f for A becomes complex and can be expressed by

$$f_A(Q,E) = f_A^o(Q) + f_A'(E) + i f_A''(E) \qquad (3)$$

where f_A° corresponds to the usual atomic scattering factor of A at an energy sufficiently away from the absorption edge of A, and f_A' and f_A'' are the real and imaginary parts of the anomalous dispersion terms of A. Using the difference of the scattering intensities in absolute units measured at two energies E_1 and E_2 on the lower energy side of the absorption edge of A (which are 300 and 25 eV below the corresponding edge in the present AXS measurements), the differential interference function around A, Δi_A is given by

$$\begin{aligned}\Delta i_A(Q,E_1,E_2) &= \frac{(I_{eu}(Q,E_1) - \langle f^2(Q,E_1)\rangle) - (I_{eu}(Q,E_2) - \langle f^2(Q,E_2)\rangle)}{W(Q,E_1,E_2)} \\ &= \frac{x_A(f_A'(E_1) - f_A'(E_2))}{W(Q,E_1,E_2)} \int_o^\infty 4\pi r^2 \sum_{j=1}^N \Re[f_j(Q,E_1) + f_j(Q,E_2)] \\ &\quad \times (\rho_{Ni\,j}(r) - \rho_{oj}) \frac{\sin(Qr)}{Qr} dr \end{aligned} \qquad (4)$$

$$W(Q,E_1,E_2) = \sum_{j=1}^N x_j \Re[f_j(Q,E_1) + f_j(Q,E_2)] \qquad (5)$$

where $\rho_{Aj}(r)$ is the radial distribution function of the element j around A and $\rho_{o,j}$ the average number density of the element j. $\Re$ denotes the real part of the values in the brackets. Eq.(4) suggests that the differential interference functions of Δi_A enables us to provide the structural information around Ni alone. Thus, the Fourier transformation of eq.(4) gives the environmental RDF for A.

$$4\pi r^2\rho_o + \frac{2r}{\pi x_A\left(f'_A(E_1)-f'_A(E_2)\right)}\int_0^\infty Q\Delta i_A(Q,E_1,E_2)\,\sin(Qr)\,dQ \qquad (6)$$
$$= 4\pi r^2 \sum_{j=1}^{n} \frac{\Re\left[f_j(Q,E_1)+f_j(Q,E_2)\right]}{W(Q)}\,\rho_{Aj}(r)$$

III. Results and Discussion

Amorphous $La_{55}Al_{25}Ni_{20}$ alloys[13]

The ordinary interference functions $Qi(Q)$ of the as-quenched sample and the sample annealed for 300 s at 510 K in the supercooled liquid region are compared in the top of **Fig.1** and their difference is shown in the curve (a) of the same figure. Only the differences (b) and (c) are shown for the samples annealed for 1.8 ks at 488 K just above T_g and for 10.8 ks at 418 K below T_g. These intensity differences show an almost identical profile in spite of the annealing conditions. It is surprising that the structural change due to annealing below T_g is identical to those due to annealing in the supercooled liquid region. Of course, since our measurements with x-ray diffraction were carried out at room temperature, the interference functions in Fig.1 do not describe the structure at the elevated temperature for annealing. However, the result in Fig.1 suggests an important implication that no chemical rearrangement of the constituent elements accompanied with long-range atomic diffusion occurs due to low temperature annealing not only at a temperature below T_g but also in the supercooled liquid region. This indicates that there may be no difference between the structural variation in the sample annealed in the supercooled liquid region above T_g and the structural variation resulting from the irreversible structural relaxation below T_g. These identical profiles of the intensity differences in Fig.1 also demonstrate the thermal stability of the present amorphous alloy.

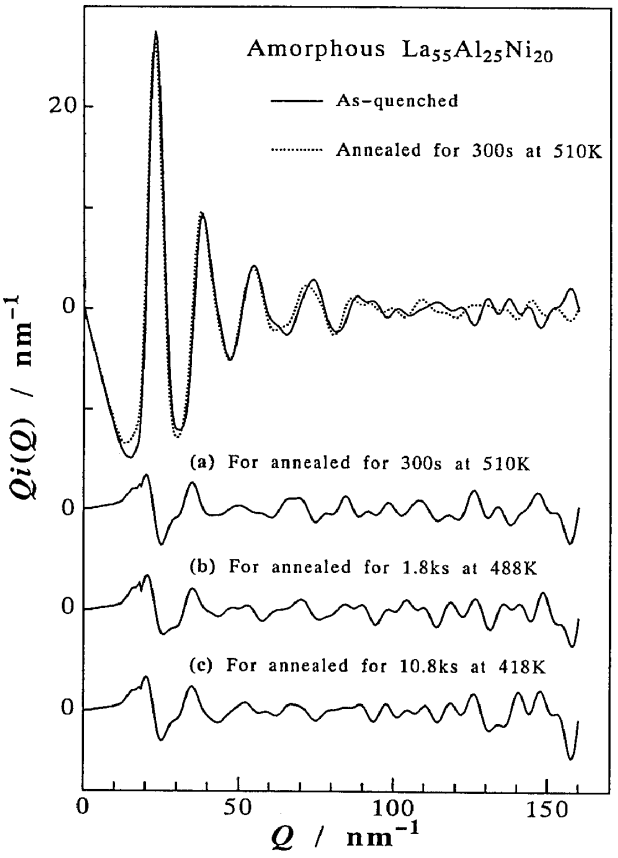

Figure 1 Differences of interference functions of $La_{55}Al_{25}Ni_{20}$ amorphous alloys between the indicated annealed samples and the as-quenched sample (curves a, b and c).

The ordinary RDF and the environmental RDF for Ni of the $La_{55}Al_{25}Ni_{20}$ amorphous alloy are shown in **Fig.2 a** and **b**, respectively. The solid and dotted curves in the figure correspond to the as-quenched sample and the sample annealed for 300 s at 510 K in the supercooled liquid region. As expected from the interference function in Fig.1, the

RDFs of both the amorphous samples show an almost identical pattern. The first peak at r_1 has a shoulder at r_2 in the ordinary RDF. The first peak in the environmental RDF for Ni consists of only a single peak at r_1 and no peak is observed at r_2. Since the environmental RDF for Ni is a sum of the three partial RDFs of Ni-Ni, Ni-La and Ni-Al pairs, the peak at r_1 is attributed to any of these pairs including Ni and the peak at r_2 to any of the others without Ni of La-La, La-Al and Al-Al pairs.

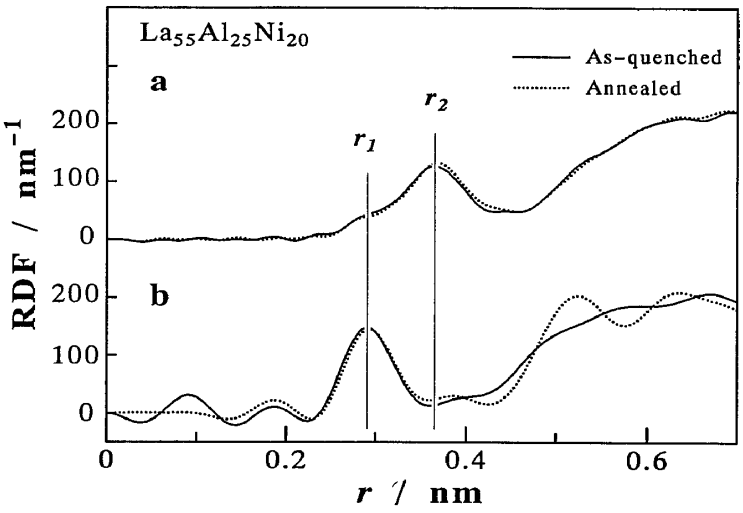

Figure 2 The ordinary RDFs (curve a) and the environmental RDFs for Ni (curve b) in $La_{55}Al_{25}Ni_{20}$ amorphous alloys as-quenched and annealed 300 s at 510 K.

The area under the peak for *j-k* pairs in the ordinary RDF, A_{jk} is related with the coordination number of the atom *k* around the atom *j*, N_{jk} at an average distance r_{jk} which is given by the position of the peak, that is

$$A_{jk} = \int_a^b 4\pi r^2 \rho(r)\, dr = \frac{x_j f_j f_k}{(\sum_{i=1}^{N} x_i f_i)^2} N_{jk} \qquad (7)$$

Similarly, the area under the peak for A-*k* pairs in the environmental RDF for A, A_{Ak} is related with the coordination number of the atom *k* around A, N_{Ak}.

$$A_{Ak} = \int_a^b 4\pi r^2 \rho_A(r)\, dr = \frac{\Re[f_k(Q,E_1) + f_k(Q,E_2)]}{W(Q)} N_{Ak} \qquad (8)$$

where the values of *a* and *b* are the lower and upper limits of the peak. Using eqs. (7) and (8), the contribution of each pair to the RDFs is evaluated by computing the coefficients which are the function of the x-ray atomic scattering factor and the atomic concentration of the corresponding element. The coefficient for La-Ni pairs is about 14 times larger than those for Ni-Ni and Ni-Al pairs in the ordinary RDF of $La_{55}Al_{25}Ni_{20}$ amorphous alloy and the coefficient for Ni-La pairs is about 4 times larger than those for Ni-Ni and Ni-Al pairs in the environmental RDF. Thus, the peak at r_1 in Fig.2 is ascribed to La-Ni pairs. Namely, by carefully checking the values of the coefficients of each pair and the existence of the peaks in the ordinary and environmental RDFs, the peaks in the RDFs are often attributed to a certain pair even in the multi-component system. The values of the coefficients of La-La, La-Al and Al-Al pairs are 1.19, 0.40 and 0.02, respectively. Thus, the peak at r_2 is attributed to La-La and La-Al pairs. From the present study alone, the contributions of these two pairs cannot separately be determined.

Table 2 Coordination numbers and atomic distances of the $La_{55}Al_{25}Ni_{20}$ amorphous alloys.

	r_1 / nm	N_{LaNi}	r_2 / nm	N_{LaLa}	r_3 / nm	N_{LaNi}
As-quenched	0.283±0.002 0.287±0.002	1.5±0.1 1.4±0.1	0.358±0.002	9.4±0.5		
Annealed for 300 s at 510 K	0.284±0.002 0.290±0.002	1.5±0.1 1.4±0.1	0.362±0.002	9.8±0.5		
Crystallized (Annealed for 360 ks at 510 K)	0.284±0.002 0.299±0.002	1.2±0.1 1.2±0.1	0.360±0.002	9.8±0.5	0.402±0.002 0.385±0.002	0.8±0.1 0.8±0.1

However, since the coefficient of La-La pairs is about 3 times larger than that of La-Al pairs in the present system, it is assumed that the peak at r_2 is attributed to La-La pairs. Then, the coordination numbers and atomic distances for the peaks at r_1 and r_2 in **Table 2** were estimated by fitting these first peaks in Fig.2 with Gaussian's. The structural parameters at r_1 determined from both of the RDFs appear to agree with each other. This justifies the present AXS analyses.

The ordinary RDF and the environmental RDF around Ni of the fully crystallized $La_{55}Al_{25}Ni_{20}$ alloy are shown in **Fig.3**. The profile in the near-neighboring region is different from that of the amorphous phase in Fig.2. At r_3 in Fig.3, an additional shoulder appears in the ordinary RDF and an extrapeak is observed in the environmental RDF around Ni. In **Fig.4**, the scattering profile of the crystallized sample measured with Cu Kα-radiation is compared with the peak positions of several La-Ni and La-Al metallic compounds[14]. All compounds except La_3Ni explain some of the observed peaks although a satisfactory match between them has not been accomplished yet. However, it is likely that the atomic structures of the crystallized sample is close to these compounds. From the calculation of atomic distances of La_7Ni_3 and LaNi[15], it is found that the peak at r_3 corresponds to the second nearest-neighbor distance of La-Ni pairs. Thus, the coordination number at r_3 is estimated as the second neighboring La-Ni pairs. The coordination numbers at r_1 and r_3 in Fig.3 give satisfactory agreement in both of the RDFs as seen in Table 2. However, the differences between the atomic distances at r_1 and r_3 in both RDFs of the crystallized sample is much larger than the one in the amorphous samples. This may result from the unsatisfactory understanding of the crystalline phase of the precipitates in the crystallized sample.

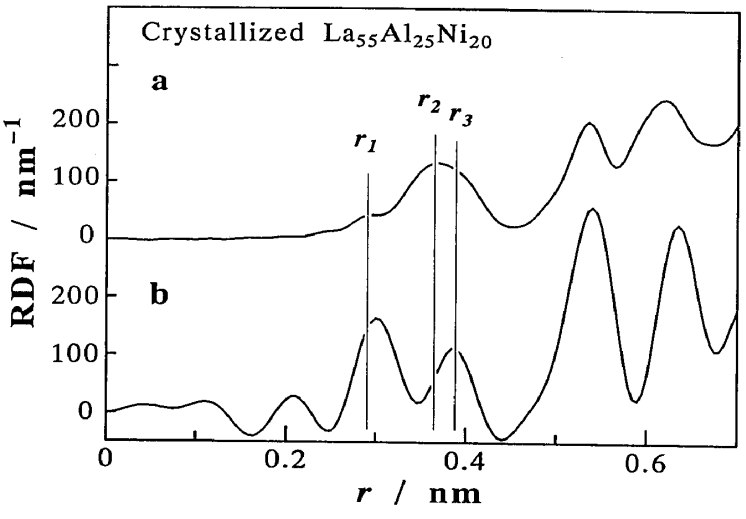

Figure 3 The ordinary (curve a) and environmental RDFs for Ni (curve b) of $La_{55}Al_{25}Ni_{20}$ crystallized by annealing 360 ks at 510 K (5.90 Mg/m^3).

From the coordination

numbers of La-Ni and La-La pairs in the amorphous samples in Table 2, it is noted that the number of La around La is much larger than the number expected from the concentration of La. This implies that the random distribution of atoms is not well-recognized in these amorphous alloys. Although no significant change of the structure parameters due to low-temperature annealing is observed in the amorphous alloys, the coordination number of Ni around La at the nearest-neighbor distance slightly decrease and the new peak which may be attributed to the second neighboring La-Ni pairs appears in the crystallized sample. These experimental results suggest that La atoms must be rearranged around Ni atoms for crystallization. Thus, the diffusion of La atoms around Ni may control the crystallization process and as a result, good thermal stability in this amorphous alloy may be provided.

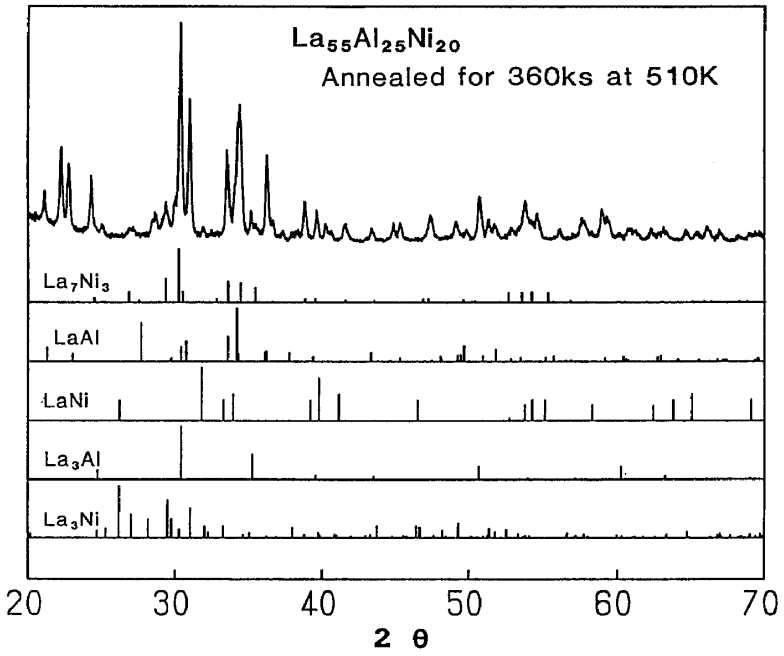

Figure 4 Scattering intensity profile of the crystallized $La_{55}Al_{25}Ni_{20}$ alloy is compared with the peak positions of some La-Ni and La-Al compounds.

Amorphous $Zr_{60}Al_{15}Ni_{25}$ alloys

The differential interference functions for Zr, $Q\Delta i_{Zr}$ in the $Zr_{60}Al_{15}Ni_{25}$ alloys which is defined in eq.(4) are shown in **Fig.5**. The solid and dotted curves in Fig.5 (a) correspond to the as-quenched amorphous alloy and the amorphous alloy annealed for 120 s at 730 K, and the solid curve in Fig.5 (b) to the crystallized sample by annealing for 180 ks at 730 K. Similarly, the differential interference functions for Ni, $Q\Delta i_{Ni}$ are shown in **Fig.6**. No large difference between the differential interference functions of the as-quenched and annealed amorphous alloys for Zr and Ni are observed. In the function $Q\Delta i_{Zr}$ the profile of the

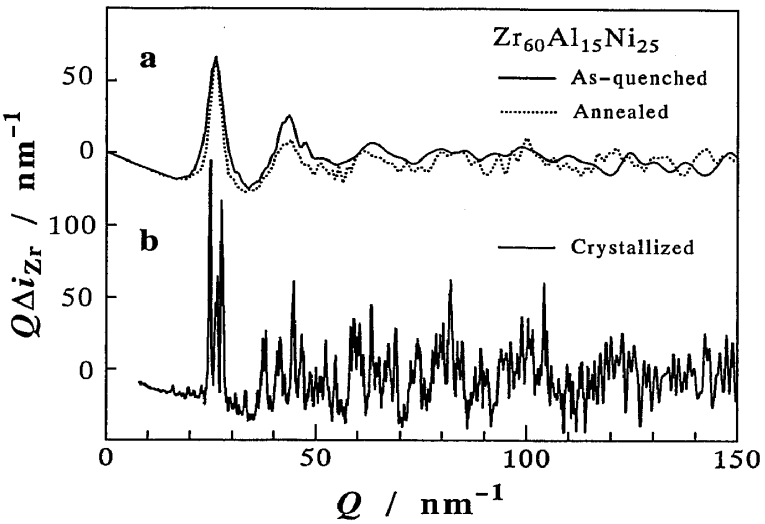

Figure 5 Differential interference functions for Zr of as-quenched, annealed and crystallized $Zr_{60}Al_{15}Ni_{25}$ amorphous alloys.

annealed sample becomes slightly sharper than that of the as-quenched sample.

The curves a, b and c in **Fig.7** correspond to the ordinary RDF and the environmental RDFs for Zr and Ni of the $Zr_{60}Al_{15}Ni_{25}$ amorphous alloy, respectively. The solid and dotted curves correspond to the as-quenched sample and the sample annealed for 120 s at 730 K. The first peak at r_2 in the ordinary RDF has a shoulder at r_1 in Fig.7. The profile of the first peak in the

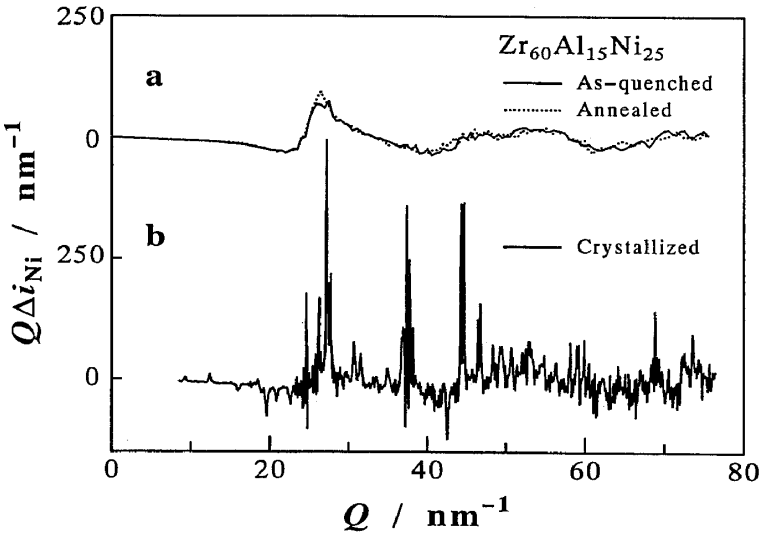

Figure 6 Differential interference functions for Ni of as-quenched, annealed and crystallized $Zr_{60}Al_{15}Ni_{25}$ amorphous alloys.

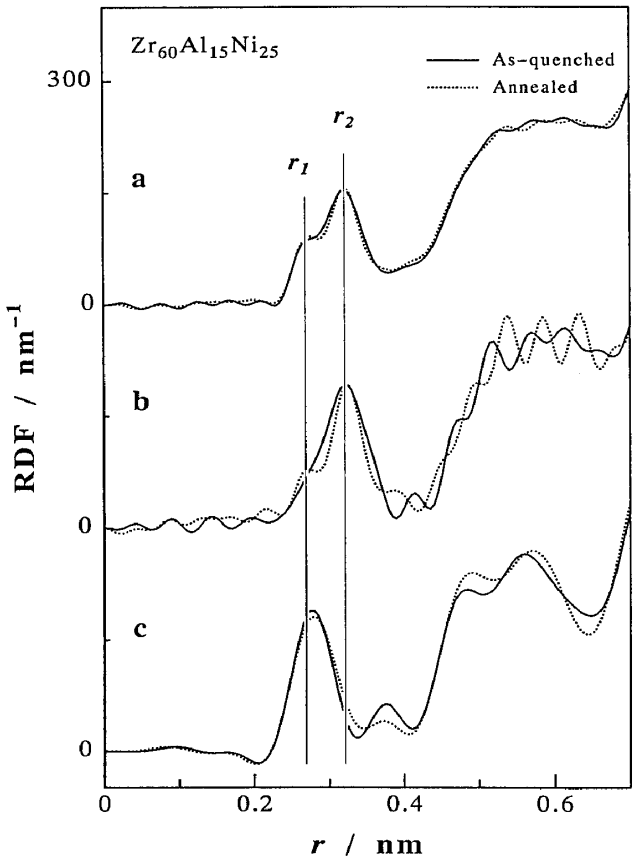

Figure 7 The ordinary (curves a) and environmental RDFs for Zr (curves b) and for Ni (curves c) of $Zr_{60}Al_{15}Ni_{25}$ amorphous alloys.

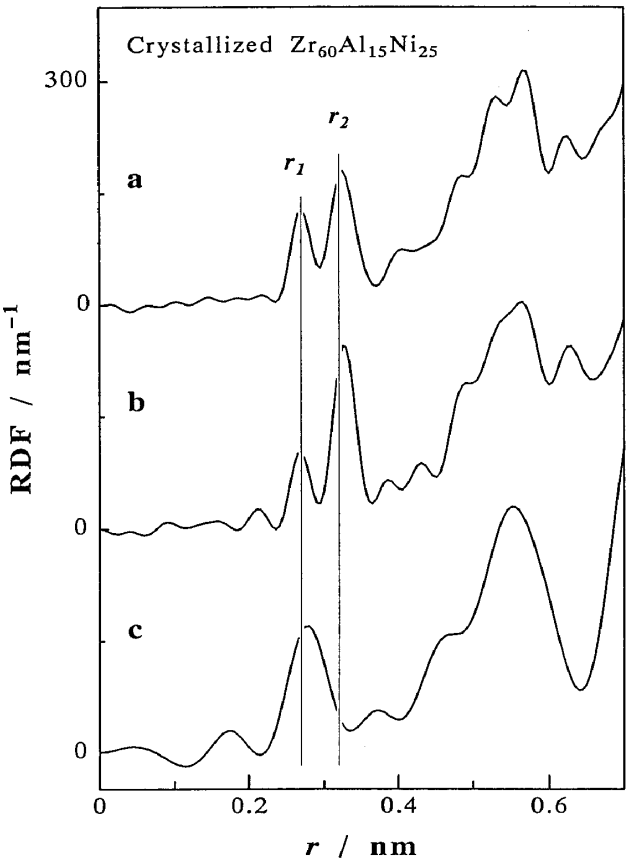

Figure 8 The ordinary (curves a) and environmental RDFs for Zr (curves b) and for Ni (curves c) of the crystallized $Zr_{60}Al_{15}Ni_{25}$ alloy.

environmental RDF for Zr is similar to that in the ordinary RDF. On the other hand, in the environmental RDF for Ni, the first peak at r_1 does not have any shoulder on either side of the peak and no peak exists at r_2. By the similar discussion to the one in the RDFs of Fig.2 for the $La_{55}Al_{25}Ni_{20}$ amorphous alloys based on the definition of the environmental RDFs in eq.(6), the atomic radius of each element (Zr:0.160 nm, Al:0.143 nm and Ni:0.124 nm) and the values of the coefficients of the RDF in eqs.(7) and (8), the peak at r_1 is attributed to Zr-Ni pairs and the peak at r_2 to Zr-Al and Zr-Zr pairs. By fitting the first peak of the ordinary RDF and the environmental RDF for Zr with two Gaussian profiles at r_1 and r_2, and the first peak of the environmental RDF for Ni with a Gaussian profile at r_1, the areas and the positions of the peaks at r_1 and r_2 were computed. From the area of the peak at r_1, the coordination number of Ni around Zr, N_{ZrNi} was directly estimated using the eqs.(7) and (8). Both of the areas of the peaks at r_2 including Zr-Al and Zr-Zr pairs in the ordinary RDF in eq.(7) and in the environmental RDF for Zr in eq.(8) were solved for the coordination numbers of N_{ZrAl} and N_{ZrZr}. The ordinary RDF and the environmental RDFs for Zr and Ni in the crystallized $Zr_{60}Al_{15}Ni_{25}$ alloy are shown in **Fig.8**. The peaks at r_1 and r_2 becomes sharper in the crystalline sample and the shoulders at r_1 in the curves a and b in Fig.7 become isolated peaks in Fig.8. The coordination numbers at r_1 and r_2 are similarly calculated. All the structural parameters at r_1 and r_2 for these three samples are summarized in **Table 3**. The structural parameters at r_1 for the as-quenched and annealed

Table 3 Coordination numbers and atomic distances of the $Zr_{60}Al_{15}Ni_{25}$ amorphous alloys.

		r_1 / nm	N_{ZrNi}	r_2 / nm	N_{ZrZr}	N_{ZrAl}
As-quenched	RDF	0.267±0.002	2.3±0.2	0.317±0.002	10.3±0.7	-0.1±0.9
	RDF_{Zr}	0.267±0.002	2.1±0.5			
	RDF_{Ni}	0.269±0.002	2.3±0.2			
Annealed for 120 s at 730 K	RDF	0.268±0.002	2.5±0.2	0.318±0.002	8.9±1.0	1.0±0.8
	RDF_{Zr}	0.267±0.002	2.3±0.5			
	RDF_{Ni}	0.271±0.002	2.4±0.2			
Crystallized (Annealed for 180 ks at 730 K)	RDF	0.268±0.002	3.0±0.2	0.322±0.002	8.2±0.9	0.8±0.7
	RDF_{Zr}	0.267±0.002	3.0±0.5			
	RDF_{Ni}	0.273±0.002	2.3±0.2			

amorphous samples determined by the three different RDFs in Fig.7 coincide with each other within the experimental errors, which verifies the present AXS analyses and supports the experimental result that the peak at r_1 is attributed to Zr-Ni pairs. However, in the crystallized sample of Fig.8, the coordination numbers of N_{ZrNi} at r_1 obtained from the environmental RDF for Ni is much smaller than those from the ordinary RDF and the environmental RDF for Zr. This difference could be explained as follows.

Let me consider that the area at r_1 in the environmental RDF for Zr may include not only the contribution of Zr-Ni pairs but also some additional pairs which are not attributed to the peak at r_1 in the environmental RDF for Ni. Though these pairs are Zr-Al and Zr-Zr pairs, the atomic distances of Zr-Al (0.303 nm) and Zr-Zr pairs (0.320 nm) calculated from the Goldschmidt radii are larger than the peak position of about 0.27 nm. The peak positions in the scattering profile of the crystallized sample measured with Cu Kα-radiation are compared with the peak positions of some Zr-Al and Zr-Ni compounds[14] in **Fig.9**. As seen in the figure, all the compounds ZrNi, Zr_2Ni, ZrAl and Zr_3Al_2 appear to explain the experimental data quite well. Although the precipitation phases cannot be specified from the present data alone, it must be noted that the average nearest neighbor distances for Zr-Al pairs in ZrAl and Zr_3Al compounds calculated from their atomic structures[15] are 0.280 and 0.275 nm, respectively. These distances are much shorter than the distance (0.303 nm) calculated from the Goldschmidt

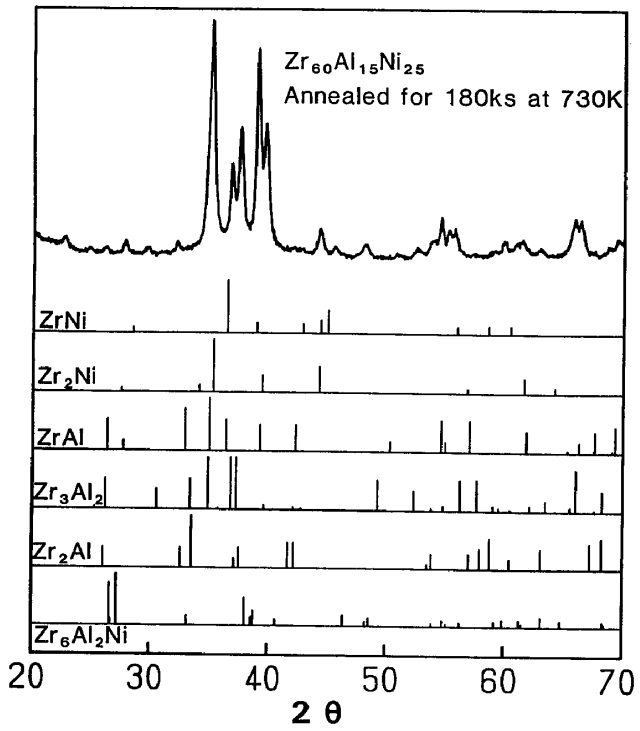

Figure 9 Scattering intensity profile of the crystallized $Zr_{60}Al_{15}Ni_{25}$ alloy is compared with the peak positions of some Zr-Ni and Zr-Al compounds.

Table 4 Atomic fractions of the constituent elements in the nearest neighboring shell around Zr.

	As-quenched	Annealed for 120 s at 730K	Crystallized (Annealed for 180 ks at 730K)
Zr-Zr	82%	72%	63%
Zr-Ni	18%	20%	18%
Zr-Al	0%	8%	20%

radii, which indicates that the atomic distance of Zr-Al pairs is shorter in the crystallized sample than in the amorphous samples. Therefore, it is assumed that the peak at r_1 in the environmental RDF for Zr may include Zr-Al pairs as well as Zr-Ni pairs. Using the coordination number for Zr-Ni pairs of 2.3 which was estimated from the area under the peak at r_1 in the environmental RDF for Ni, the coordination number of Al around Zr, N_{ZrAl} is estimated from the area at r_1 in the environmental RDF for Zr to be 1.8 with the value of 2.3 for N_{ZrNi} at r_1 in the crystallized sample. The coordination numbers of Zr-Zr and Zr-Al pairs at r_2 in the crystallized sample are also calculated with the method explained above. It is also found in Table 3 that the coordination number of N_{ZrZr} at r_2 decreases with the annealing time while the coordination number of N_{ZrAl} at r_2 increases with time.

The atomic distance between Zr-Ni pairs of about 0.268 nm on an average in Table 3 is much less than the distance of 0.284 nm calculated from the Goldschmidt radii, which may imply the presence of the strong bonding between Zr and Ni. The atomic distance between Zr-Zr pairs of 0.317 to 0.322 nm in Table 3 is almost equal to the distance of 0.320 nm obtained from the Goldschmidt radii. Since the correlation distance between the different kinds of atoms are shorter than the distance expected from the Goldschmidt radii. Thus, using the coordination numbers of N_{ZrZr}, N_{ZrAl} and N_{ZrNi} in the nearest neighbor pairs in Table 3, the total coordination numbers around Zr are estimated to be 12.5, 12.3 and 13.1 for the as-quenched, annealed and crystallized samples, respectively, and the fraction of each constituent element around Zr can be calculated. The obtained fractions are summarized in **Table 4**. It is found from this table that the fractions of Ni atoms around Zr do not change by annealing, the fractions of Zr atoms around Zr gradually decrease with annealing time, and only the fractions of Al atoms around Zr show a sudden increase in the crystallized sample. Taking account of these experimental data, especially the drastic change of the fraction of Al atoms around Zr and the appearance of Zr-Al pairs with shorter atomic distance in the crystallized sample, it seems that the Al atoms must be rearranged around Zr atoms for crystallization, which may retard the crystallization in the present systems. Inoue *et al.*[5] have already pointed out the effectiveness of Al addition in Zr-Ni binary system on high thermal stability in the Zr-Al-Ni amorphous alloy. The present result provides the experimental evidence for their discussion.

IV. Summary

Some additional quantitative structural analyses, including the complete determination of the

crystalline phase, are progressing for further understanding of the amorphous alloys with a wide supercooled liquid region. However, in the present study, some suggestive results were obtained. For the crystallization of these amorphous alloys, the environmental structure around a certain element is largely changed. Such as, Ni atoms around La in the $La_{55}Al_{25}Ni_{20}$ amorphous alloy and Al atoms around Zr in the $Zr_{60}Al_{15}Ni_{25}$ amorphous alloy. As pointed out by Inoue *et al.*[2,3,5] from the glass-forming capacity and the equilibrium phase diagram, there exists strong bonding between the different kinds of atoms in the alloys. This strong bonding and the drastic change of the environmental structure around a certain element required for crystallization may thermally stabilize the amorphous alloys by retarding the crystallization.

Acknowledgement

The authors want to thank Prof.M.Nomura, Photon Factory, National Laboratory for High Energy Physics for his kind help on the AXS measurements (Proposal No.90-091).

References

1. H.S.Chen and K.A.Jackson, *Metallic Glasses*, ASM, Metals Park, Ohio, (1978), p.75.
2. A.Inoue, T.Zhang and T.Masumoto, *Mater. Trans. Japan Inst. Metals*, **30** (1989), 965.
3. A.Inoue, H.Yamaguchi, T.Zhang and T.Masumoto, *Mater. Trans. Japan Inst. Metals*, **31** (1990), 104.
4. H.S.Chen and A.Inoue, *J. Non-Cryst. Solids*, **61/62** (1984), 805.
5. A.Inoue, T.Zhang and T.Masumoto, *Mater. Trans. Japan Inst. Metals*, **31** (1990), 177.
6. C.N.J.Wagner, H.Ocken and M.L.Joshi, *Zeit. Naturforsch.*, **20a** (1965), 325.
7. International Tables for X-ray Crystallography, Vol.IV, Kynoch, Birmingham 1974, p.99 and 149.
8. D.T.Cromer and J.B.Mann, *J. Chem. Phys.*, **47**, (1967), 1892.
9. Y.Waseda, *Novel Application of Anomalous X-ray Scattering for Structural Characterization of Disordered Materials*, Springer-Verlag, Heidelberg, (1984), p.75.
10. D.T.Cromer and D.Liberman, *J. Chem. Phys.*, **53**, (1970), 1891.
11. Y.Waseda, E.Matsubara and H.Ohta, *High Temp. Mater. Proc.*, **8**, (1988), 61.
12. E.Matsubara, K.Harada, Y.Waseda and M.Iwase, *Zeit. Naturforsch.*, **44a**, (1988), 723.
13. E.Matsubara, T.Tamura, Y.Waseda, T.Zhang, A.Inoue and T.Masumoto, Proc. 5th Int. Conf. on the Structure of Non-Crysatlline Materials, Sep.2-6, 1991, Sendai. p.95.
14. Joint Committee on Powder Diffraction Standards.
15. P.Villars and L.D.Calvert, *Pearson's Handbook of Crystallographic Data for Intermetallic Phases, Vol.3*, ASM, Metals Park, Ohio, (1985).